Calphad 64 (2019) 205–212

Contents lists available at ScienceDirect

Calphad

journal homepage: www.elsevier.com/locate/calphad

Thermodynamic assessment of the Co-Ta system

Peisheng Wang[a,*], Jörg Koßmann[b], Ursula R. Kattner[c], Mauro Palumbo[b], Thomas Hammerschmidt[b], Gregory B. Olson[a]

[a] Center for Hierarchical Materials Design (CHiMaD), Northwestern University, 2205 Tech Drive, Evanston, IL 60208, United States
[b] Interdisciplinary Centre for Advanced Materials Simulation (ICAMS), Ruhr-Universität Bochum, 44801 Bochum, Germany
[c] Materials Science and Engineering Division, National Institute of Standards and Technology, 100 Bureau Dr., MS 8555, Gaithersburg, MD 20899, United States

ARTICLE INFO

Keywords:
TCP phase
γ-γ'
Co-based superalloys
CALPHAD

ABSTRACT

The Co-Ta system has been reviewed and the thermodynamic description was re-assessed in the present work. DFT (density functional theory) calculations considering spin polarization were performed to obtain the energies for all end-member configurations of the C14, C15, C36 and μ phases for the evaluation of the Gibbs energies of these phases. The phase diagram calculated with the present description agrees well with the experimental and theoretical data. Considering the DFT results was essential for giving a better description of the μ phase at lower temperatures.

1. Introduction

The efficiency of gas turbines increases with increasing turbine inlet temperature. The hot zones of the gas turbines are often made from Ni-based superalloys. However, Ni-based superalloys are reaching the upper limit for further temperature increases imposed by the melting point of Nickel [1]. The higher melting point of Co compared to Ni makes Co-based alloys attractive candidates for extending the application of these alloys to higher temperatures. A limiting factor for the application of traditional Co-based alloys is their relative low strength compared to Ni-based superalloys. The primary strengthening mechanism for single crystal Ni-based superalloys is precipitation strengthening. The geometrically close packed γ'-Ni_3Al phase with an $L1_2$ ordered FCC (face centered cubic) lattice precipitates in a γ phase matrix (FCC_A1) [2]. However, in the Co-Al binary system, the $L1_2$-Co_3Al phase is not a stable phase. Sato et al. [3] found that a γ' phase with $L1_2$ structure forms in the Co-Al-W system and showed that as a result of the precipitation of γ' in a γ matrix the high-temperature strength of these alloys was significantly increased. However, subsequent investigations have revealed that the γ' phase is metastable and additional elements, such as Ti, Ta, Hf, Nb and Ni [4], are needed to stabilize the γ' phase [5]. Although the $L1_2$-Co_3Ta phase is also metastable, density functional theory (DFT) calculations have shown that the enthalpy of formation of $L1_2$-Co_3Ta with −21.90 kJ/mol (mole of atoms) [6] is fairly negative. In addition, Ta shows the strongest effects for increasing the γ' solvus temperature among the reported elements [4]. These are strong indicators to use Ta for the stabilization of the γ' phase in Co-Al-W based alloys. On the other hand, topologically close packed (TCP) phases, C14, C15, C36 and μ phases, which are detrimental to the alloy properties are stable phases in the Co-Ta system. The stability of these phases arises from the in total half-full d-band and the difference in atomic size [7]. Thus, accurate knowledge of the homogeneity ranges of these TCP phases is critical for the addition of Ta to Co-based alloys.

CALPHAD (CALculation of PHAse Diagrams) simulations are widely accepted as an effective way for accelerated development of new alloys [8]. The availability of a high quality thermodynamic description of the Co-Ta system is key for the development of a reliable multi-component thermodynamic database for superalloys. However, the thermodynamic descriptions for the Co-Ta from literature do not fully meet this requirement.

2. Literature review

The solid phases occurring in this binary system are summarized in Table 1 [9]. Thermodynamic assessments of the Co-Ta system were carried out by Liu et al. [10], Hari Kumar et al. [11] and Shinagawa et al. [12]. Shinagawa et al. [12] experimentally investigated the phase equilibria in the Co-Ta system and significantly revised the phase boundaries for the TCP phases which were used for the development of a new thermodynamic description. The thermodynamic descriptions from Liu et al. [10] and Hari Kumar et al. [11] were based on a previous version of the phase diagram and do not reproduce the experimental phase diagram from Shinagawa et al. [12]. Although the description

* Corresponding author.
E-mail address: peisheng.wang@outlook.com (P. Wang).

https://doi.org/10.1016/j.calphad.2018.12.002
Received 12 October 2018; Received in revised form 29 November 2018; Accepted 2 December 2018

Table 1
Summary of the crystallographic information for the phases of the Co-Ta system [9].

Phase name	Crystallographic information			
	Strukturbericht.	Prototype	Pearson symbol	Space group
Observed stable and metastable phases				
FCC, γ or αCo	A1	Cu	cF4	Fm-3 m
HCP, εCo	A3	Mg	hP2	*P63/mmc*
(Ta)	A2	W	cI2	Im-3 m
Co_3Ta		$BaPb_3$	hR12	R-3 m
C36	C36	$MgNi_2$	hP24	*P63/mmc*
C15	C15	Cu_2Mg	cF24	Fd-3 m
C14	C14	$MgZn_2$	hP12	*P63/mmc*
μ	$D8_5$	Fe_7W_6	hR13	R-3 m
C16	C16	Al_2Cu	tI12	I4/mcm
$L1_2$	L12	Cu_3Au	cP4	Pm-3 m
Hypothetical phases				
A15	A15	Cr_3Si	cP8	Pm-3n
χ	$D0_{19}$	Ni_3Sn	hP8	*P63/mmc*
σ	$D8_b$	σCrFe	tP30	$P4_2/mnm$

from Shinagawa et al. [12] reproduces the experimental phase diagram well, the calculated enthalpies of formation are significantly different from the results from DFT calculations which implies that the Gibbs energy values of the entire Co-Ta system from this description may not be reliable.

The phase diagram of the Co-Ta system has been subject to several experimental investigations. In addition to the three terminal solid solutions, FCC-Co, HCP-Co (hexagonal close packed) and BCC-Ta (body centered cubic) a number of intermetallic phases have been reported. Haschimoto [13] and Köster et al. [14] investigated the Co-rich side of the Co-Ta system using thermal analysis. Korchynsky and Fountain [15] used optical metallography and X-ray diffraction (XRD) to study the Co-rich side of the system and found four stable and one metastable intermetallic compounds. They reported the existence of the three Laves phases. The two new phases they found were a metastable Co_3Ta phase with $L1_2$ structure which on continued aging transformed into a stable Co_3Ta phase with hexagonal structure. In their study of the Co-rich side, Dragsdorf and Forgeng [16] observed the same phases and found that the structure of the Co_3Ta phase is related to the C36 structure. The structure of this phase was identified by Ponsionen and Van Vucht [17] as $BaPb_3$ type. Raman [18] examined alloys with compositions from an atomic fraction of 20% Ta to 90% Ta that were annealed at 1000 °C and 1300 °C. He confirmed the occurrence of phases with C14, C15, C36 structure and found two new phases, $CoTa_2$ with C16 structure and Co_6Ta_7 with the structure of the μ phase ($D8_5$). Pet'kov et al. [19] investigated the Co-Ta system by differential thermal analysis (DTA) and optical microscopy. They placed the Co_3Ta phase at an atomic fraction of 22% Ta. This composition was later confirmed by Xu et al. [20] and Shinagawa et al. [12]. Bernard et al. [21] used thermal analysis and optical microscopy to investigate the Ta-rich side of the system. These investigations are the basis for the phase diagram published in the compilation by Massalski et al. [22]. In this compilation the Co_3Ta phase is labeled Co_7Ta_2 although its ideal stoichiometry was placed at Co_3Ta in the work by Dragsdorf and Forgeng [16] and Ponsionen and Van Vucht [17]. Itoh et al. [23] studied the homogeneity ranges and magnetic properties of the three Laves phases C36, C15 and C14 in the Co-Ta system by XRD, density and magnetometric measurements. The composition range of C36 and C15 were determined through XRD while for the C14 phase only an approximate composition was reported. Shinagawa et al. [12] studied the entire composition range the Co-Ta system using annealed alloys and diffusion couples with XRD, scanning electron microscopy (SEM), electron probe microanalyzer (EPMA) and DTA. The homogeneity ranges and thermal stabilities for the three Laves phases (C15, C36, C14), Co_3Ta, μ phase and $CoTa_2$ (C16) phase have been determined between 1173 K and 1723 K. Shaipov et al. [24] determined the phase equilibria of the Co-Ta system in a diffusion couple at 1375 K and alloys annealed at 1200 K and at 1375 K. However, the homogeneity ranges obtained by Shaipov et al. [24] for the μ and C16 phases in the annealed alloys and the diffusion couple are not consistent, hence these data were not included for thermodynamic optimization in the present work.

In the present work, the experimental results from Shinagawa et al. [12] are considered the most accurate data set. The experimental data from [15,21] show large deviations from the evaluated phase diagram and were excluded during optimization of the present description.

3. Thermodynamic modeling

3.1. Pure elements

The descriptions of the Gibbs energy of the pure elements as function of temperature $G_{Co}^{HSER,\varphi}$ and $G_{Ta}^{HSER,\varphi}$, are taken from the pure element thermodynamic database of the Scientific Group Thermodata Europe (SGTE) [25]. For Co and Ta the data in this database are identical to those compiled by Dinsdale [26].

3.2. Solution phases

The composition dependence of the Gibbs energy of the solution phases: φ (liquid), (Ta) (BCC_A2), (αCo) (FCC_A1), (εCo) (HCP_A3) is described by a substitutional solution model with Redlich–Kister polynomials [27]. The magnetic contribution to the Gibbs energy of the solution phase is described with the Hillert-Jarl formalism [28]. In this formalism the magnetic transformation temperature and magnetic moment are the input parameters to describe the temperature dependence. The composition dependence can also be described with Redlich-Kister polynomials.

3.3. Intermetallic compounds

The uncertainty regarding the composition of the Co_3Ta phase which resulted in it being also labeled Co_7Ta_2 and the observations by Xu et al. [20] at 1223 K and Shinagawa et al. [12] at 1273 K suggest that this phase could have a homogeneity range. However, experimental evidence supporting this is too sparse to justify modeling a homogeneity range and, therefore, it is modeled as simple stoichiometric compound with a stoichiometric ratio corresponding to the observed composition:

$$G^{Co_3Ta} = 7G_{Co}^{HSER} + 2G_{Ta}^{HSER} + \Delta G_f^{Co_3Ta} \quad (1)$$

where HSER normally stands for the reference state of the element, i.e., its stable form at 298.15 K and 1 bar. However, it must be pointed out that for the magnetic elements, such as Fe, Co and Ni, HSER stands for their paramagnetic state at 298.15 K and 1 bar. $\Delta G_f^{Co_3T\alpha} = A + B{\cdot}T$ represents the Gibbs energy of formation of the compound Co_3Ta from the components Co and Ta, referred to G_{Co}^{HSER} and $2G_{T\alpha}^{HSER}$. As mentioned above, G_{Co}^{HSER} does not include the magnetic contribution of pure HCP-Co. The composition ratio of 7:2 was chosen to better reflect the composition of this phase in the phase diagram. The parameters A and B are to be optimized.

The ordered phases C14, C15, C36, μ and C16 with homogeneity ranges, were described by the Compound Energy Formalism (CEF) [29] using the sublattices $(Co,Ta)_4(Co,Ta)_2(Co,Ta)_6$, $(Co,Ta)_2(Co,Ta)_1$, $(Co,Ta)_8(Co,Ta)_4(Co,Ta)_{12}$, $(Co,Ta)_1(Co,Ta)_4(Co,Ta)_2(Co,Ta)_6$ and $(Co,Ta)_1(Co,Ta)_2$, respectively. The chosen sublattices for the C14, C15 and C16 phases correspond to a complete representation of the respective Wyckoff positions. The sublattices for C36 and μ phase instead combine Wyckoff positions of the same coordination number (CN) (C36: 4CN16 + 4CN16, 6CN12 + 6CN12) or of similar coordination number (μ: 2CN15 + 2CN16). As the coordination number of each

neighbor polyhedron is directly related to its volume and the structural stability of the μ and Laves phases is predominantly driven by atomic size differences (see e.g. discussion in Refs. [7] and [30]), we can expect that Wyckoff sites of same or similar coordination number can be combined into one sublattice.

With the CEF the Gibbs energy for the C16 phase as example is described as:

$$\begin{aligned} G_m^{C16} &= y'_{Co}y''_{Co}G^{C16}_{Co:Co} + y'_{Co}y''_{Ta}G^{C16}_{Co:Ta} + y'_{Ta}y''_{Co}G^{C16}_{Ta:Co} + y'_{Ta}y''_{Ta}G^{C16}_{Ta:Ta} \\ &+ RT\{(y'_{Co}\ln y'_{Co} + y'_{Ta}\ln y'_{Ta}) + 2(y''_{Co}\ln y''_{Co} + y''_{Ta}\ln y''_{Ta})\} \\ &+ y'_{Co}y'_{Ta}\left(y''_{Co}\sum_{i=0}^{n} L^{C16}_{Co,Ta:Co;i}(y'_{Co}-y'_{Ta})^i \right. \\ &\left. + y''_{Ta}\sum_{i=0}^{n} L^{C16}_{Co,Ta:Ta;i}(y'_{Co}-y'_{Ta})^i\right) \\ &+ y''_{Co}y''_{Ta}\left(y'_{Co}\sum_{i=0}^{n} L^{C16}_{Co:Co,Ta;i}(y''_{Co}-y''_{Ta})^i \right. \\ &\left. + y'_{Ta}\sum_{i=0}^{n} L^{C16}_{Ta:Co,Ta;i}(y''_{Co}-y''_{Ta})^i\right) \end{aligned} \quad (2)$$

where y'_{Co} is the constituent fraction of Co in the first sublattice; $G^{C16}_{Co:Ta}$is the Gibbs energy or lattice stability of 'compound' Co_1Ta_2; and $L^{C16}_{Co,Ta:Co;i}$is the interaction parameter between Co and Ta on the first sublattice when the second sublattice is filled with *Co*. The other variables and parameters are defined analogously.

The extended Compound Energy Formalism (CEF) [31] was used to describe a configuration independent contribution to the Gibbs energy of the μ phase:

$$G_m^{\mu} = G_m^{dis}(x_i) + \Delta G_m^{\text{conf}}(y_i^{(s)}) \quad (3)$$

$$G_m^{dis}(x_i) = \sum_i x_i {}^oG_i^{\mu} + \sum_i\sum_{j>i}\sum_v x_i x_j\left(x_i - x_j\right)^v L_{i,j}^{v,\mu} \quad (4)$$

$$G_m^{\text{conf}}(y_i^{(s)}) = \sum_i\sum_j\sum_k\sum_l y_i^{(1)}y_j^{(2)}y_k^{(3)}y_l^{(4)}\Delta G^{\mu}_{i:j:k:l} + RT\sum_s a^{(s)}\sum_i y_i^{(s)}\ln y_i^{(s)} \quad (5)$$

where x_i is the overall composition of the μ phase, $y_i^{(s)}$ is the fraction of site s occupied by element i, $a^{(s)}$ is the total number of sites corresponding to site s and ${}^oG_i^{\mu}$ is the molar Gibbs energy of the pure element i (Co, Ta) in the hypothetical μ structure, referred to Co-HCP and Ta-BCC without magnetic contribution. $\Delta G^{\mu}_{i:j:k:l}$ the molar Gibbs energy of formation of the stoichiometric end-member from the pure element with the Gibbs energy ${}^oG_i^{\mu}$.

In both forms of the CEF contributions from the magnetism ΔG^{μ}_{mag} can be included in the description of the end-member compound or with the modified CEF as contribution to the Gibbs energy of the pure component, ${}^oG_i^{\mu}$. In the present work, the ΔG^{μ}_{mag} was added to the pure Co end-member configuration to give a non-linear description of the magnetic contribution to the total energy.

In the CEF model, the default Gibbs energy for any end-member component is 0 unless it is given a value. However, in the traditional CEF description allowing a value of 0 will not make sure this end-member is not stable. Thus, the parameter values for all end-member compounds must be evaluated. In contrast, in the modified CEF model, the Gibbs energy of the end-members is the formation energy with respect to the pure components with the Gibbs energy ${}^oG_i^{\mu}$ resulting in a total Gibbs energy for this end-member that is not 0 J/mol. Therefore, the evaluation of the parameter values of ${}^oG_i^{\mu}$ and $\Delta G^{\mu}_{i:j:k:l}$ of the end-member with ideal site occupation will be essential. This is particularly useful for the development of thermodynamic database for multi-component systems where the number of end-member compounds can be in the millions because it is highly unlikely that an end-member with four or more components will be stable.

The metastable ordering of the FCC phase is described using the 4 sublattice order disorder formalism [32]. The equations for the Gibbs energy described by this formalism will not be repeated here, since the description of this phase is not being discussed.

4. First-principles calculations

The crystallographic information for all the solid phases is summarized in Table 1 [9]. In the present work, the total energies for all end-members of the stable C14, C15, C16, C36 and μ phase were calculated by density functional theory. using the Vienna Ab initio Simulation Package (VASP)[1] [33,34] within a high-throughput framework [30]. We used the projector augmented wave method [35] and the generalized gradient approximation [36]. The pseudo-potential for Ta included the p semicore states in the valence. Convergence tests ensured that a plane-wave cutoff of 400 eV and Monkhorst-Pack k-point mesh [37] with a density of 0.02 Å^3 were sufficient to converge differences in the formation energy to an error of less than 1 meV/atom. We allowed for spin relaxation assuming an initial ferromagnetic spin arrangement. The structures were fully relaxed (atomic positions, cell volume and lattice vectors) until the remaining forces on the atoms were less than 0.01 eV/Å. The cohesive energy and the equilibrium volume were obtained for each structure by fitting the Birch-Murnaghan equation of state to the total energy of volumes of ± 5% of the volume after full relaxation.

The enthalpies of formation for the end-members for the μ phase $\Delta G^{\mu}_{i:j:k:l:m}$ were obtained from

$$\Delta G^{\mu}_{i:j:k:l:m} = E^{\mu}_{i:j:k:l:m} - x_{Co}E^{HCP}_{Co} - x_{Ta}E^{BCC}_{Ta} \quad (6)$$

where $E^{\mu}_{i:j:k:l:m}$, E^{HCP}_{Co} and E^{BCC}_{Ta} are the total energies for the end-member *ijklm*, pure HCP Co, and pure BCC Ta calculated with spin polarization, respectively.

In addition to the energies of the phases in the Co-Ta system the energies of all end-members of other TCP phases (A15, χ σ) and the ordered lattices of the FCC, BCC and HCP have been calculated. The DFT results are summarized in Tables 2 and 3.

4.1. Modeling the magnetism of the TCP phases

The HCP ground state structure of Co, as well as Co-rich compounds, exhibit magnetic character. Thus, it is essential to describe the magnetic contribution of the total energies for the compounds containing Co. The method to describe the Gibbs energy for the end-members using DFT results in Co systems has been discussed in our previous work [38]. A straightforward method can be used to describe the magnetic contribution using only the results from spin-polarized DFT calculations. In the present work, the same method was applied to describe the C14, C15, C36 and μ phases. It will be described here briefly for the μ phase as example.

The calculated magnetic moments of Co in μ structure and HCP structure are β^{μ}_{Co} = 1.76 μ_B/atom and β^{HCP}_{Co} = 1.69 μ_B/atom, respectively. The Curie temperature for Co in the μ phase is estimated on the basis of the Heisenberg model [39] and in assumption that the exchange integrals do not significantly change between HCP and μ phases of Co: $Tc^{\mu}_{Co}/Tc^{HCP}_{Co} \approx \beta^{\mu}_{Co}/\beta^{HCP}_{Co}$, from which the Curie temperature for the μ phase can be estimated as 1460 K. Using the Hillert-Jarl [28] formalism the contribution of the magnetism at 0 K is

$$\Delta G^{\mu}_{Co,mag} = -R\ln(\beta^{\mu}_{Co}+1)(p_0\,Tc^{\mu}_{Co}) \quad (7)$$

with p_o = 0.86034 for non-BCC phases gives $\Delta G^{\mu}_{Co,mag}$ = −10603 J/mol.

[1] Commercial products are identified in this paper for reference. Such identification does not imply recommendation or endorsement by the National Institute of Standards and Technology, nor does it imply that the materials or equipment identified are necessarily the best available for the purpose.

Table 2
Enthalpies of formation, $\Delta G^{\phi}_{i:j:k:l:m}$ in J/mol (mole of atoms) of all end-members of the stable C14, C15, C36, C16 and μ phases and metastable TCP phases (A15, σ, χ) obtained from the DFT calculations $\Delta G^{\phi}_{i:j:k:l:m}$.

Phase	Wyckoff positions					$\Delta G^{\phi}_{i:j:k:l:m}$
A15 *(6c:2a)*	Co	Co	–	–	–	9235.1
	Co	Ta	–	–	–	− 4971.8
	Ta	Co	–	–	–	− 8628.3
	Ta	Ta	–	–	–	3019.5
C14 *(4f:2a:6h)*	Co	Co	Co	–	–	16,351.1
	Co	Co	Ta	–	–	44,744.2
	Co	Ta	Co	–	–	14,697.0
	Co	Ta	Ta	–	–	77,316.8
	Ta	Co	Co	–	–	− 20,562.3
	Ta	Co	Ta	–	–	1274.7
	Ta	Ta	Co	–	–	− 20,866.0
	Ta	Ta	Ta	–	–	9670.3
C15 *(16d:8a)*	Co	Co	–	–	–	19,233.5
	Co	Ta	–	–	–	− 20,942.4
	Ta	Co	–	–	–	72,275.9
	Ta	Ta	–	–	–	11,165.5
C16 *(4a:8h)*	Co	Co	–	–	–	49,098.2
	Co	Ta	–	–	–	− 24,158.6
	Ta	Co	–	–	–	24,304.2
	Ta	Ta	–	–	–	48,196.5
C36 *(4e:4f:4f$_2$:6g:6h)*	Co	Co	Co	Co	Co	17,483.0
	Co	Co	Co	Co	Ta	49,265.0
	Co	Co	Co	Ta	Co	44,962.1
	Co	Co	Co	Ta	Ta	43,606.3
	Co	Co	Ta	Co	Co	16,120.5
	Co	Co	Ta	Co	Ta	61,239.2
	Co	Co	Ta	Ta	Co	52,341.7
	Co	Co	Ta	Ta	Ta	73,845.8
	Co	Ta	Co	Co	Co	− 6961.9
	Co	Ta	Co	Co	Ta	28,532.3
	Co	Ta	Co	Ta	Co	23,519.5
	Co	Ta	Co	Ta	Ta	28,874.1
	Co	Ta	Ta	Co	Co	270.1
	Co	Ta	Ta	Co	Ta	34,031.8
	Co	Ta	Ta	Ta	Co	26,691.5
	Co	Ta	Ta	Ta	Ta	47,782.1
	Ta	Co	Co	Co	Co	− 4633.1
	Ta	Co	Co	Co	Ta	25,543.6
	Ta	Co	Co	Ta	Co	28,547.2
	Ta	Co	Co	Ta	Ta	28,957.1
	Ta	Co	Ta	Co	Co	4622.4
	Ta	Co	Ta	Co	Ta	35,323.9
	Ta	Co	Ta	Ta	Co	29,364.0
	Ta	Co	Ta	Ta	Ta	48,330.8
	Ta	Ta	Co	Co	Co	− 21,014.0
	Ta	Ta	Co	Co	Ta	2945.6
	Ta	Ta	Co	Ta	Co	3494.6
	Ta	Ta	Co	Ta	Ta	1635.3
	Ta	Ta	Ta	Co	Co	− 19,724.7
	Ta	Ta	Ta	Co	Ta	2601.7
	Ta	Ta	Ta	Ta	Co	− 1151.4
	Ta	Ta	Ta	Ta	Ta	10,485.5
χ *(2a:8c:24g$_1$:24g$_2$)*	Co	Co	Co	Co	–	4521.8
	Co	Co	Co	Ta	–	24,163.4
	Co	Co	Ta	Co	–	− 812.3
	Co	Co	Ta	Ta	–	39,550.7
	Co	Ta	Co	Co	–	− 7770.8
	Co	Ta	Co	Ta	–	14,452.4
	Co	Ta	Ta	Co	–	− 5901.7
	Co	Ta	Ta	Ta	–	17,125.5
	Ta	Co	Co	Co	–	1344.4
	Ta	Co	Co	Ta	–	15,771.0
	Ta	Co	Ta	Co	–	− 7929.1
	Ta	Co	Ta	Ta	–	33,812.2
	Ta	Ta	Co	Co	–	− 7874.9
	Ta	Ta	Co	Ta	–	4622.8
	Ta	Ta	Ta	Co	–	− 5200.5
	Ta	Ta	Ta	Ta	–	8476.1

Table 2 (*continued*)

Phase	Wyckoff positions					$\Delta G^{\phi}_{i:j:k:l:m}$
μ *(1a:6h:2c$_1$:2c$_2$:2c$_3$)*	Co	Co	Co	Co	Co	11252.0
	Co	Co	Co	Co	Ta	9318.8
	Co	Co	Co	Ta	Co	− 1196.7
	Co	Co	Co	Ta	Ta	− 5240.1
	Co	Co	Ta	Co	Co	7061.0
	Co	Co	Ta	Co	Ta	− 7062.6
	Co	Co	Ta	Ta	Co	− 13,732.8
	Co	Co	Ta	Ta	Ta	− 23,630.4
	Co	Ta	Co	Co	Co	42,629.9
	Co	Ta	Co	Co	Ta	50,641.3
	Co	Ta	Co	Ta	Co	21,723.6
	Co	Ta	Co	Ta	Ta	31,870.8
	Co	Ta	Ta	Co	Co	40,570.0
	Co	Ta	Ta	Co	Ta	26,791.2
	Co	Ta	Ta	Ta	Co	22,128.7
	Co	Ta	Ta	Ta	Ta	6398.3
	Ta	Co	Co	Co	Co	12,325.7
	Ta	Co	Co	Co	Ta	5382.8
	Ta	Co	Co	Ta	Co	5662.9
	Ta	Co	Co	Ta	Ta	− 2757.4
	Ta	Co	Ta	Co	Co	4845.6
	Ta	Co	Ta	Co	Ta	− 15,868.9
	Ta	Co	Ta	Ta	Co	− 11,408.9
	Ta	Co	Ta	Ta	Ta	− 24,628.8
	Ta	Ta	Co	Co	Co	54,718.6
	Ta	Ta	Co	Co	Ta	60,352.7
	Ta	Ta	Co	Ta	Co	23,781.8
	Ta	Ta	Co	Ta	Ta	33,961.7
	Ta	Ta	Ta	Co	Co	53,127.5
	Ta	Ta	Ta	Co	Ta	42,368.4
	Ta	Ta	Ta	Ta	Co	26,682.9
	Ta	Ta	Ta	Ta	Ta	10,458.0
σ *(2a:4f:8i$_1$:8i$_2$:8j)*	Co	Co	Co	Co	Co	5637.7
	Co	Co	Co	Co	Ta	9033.1
	Co	Co	Co	Ta	Co	3545.0
	Co	Co	Co	Ta	Ta	2016.1
	Co	Co	Ta	Co	Co	− 6856.8
	Co	Co	Ta	Co	Ta	− 4137.3
	Co	Co	Ta	Ta	Co	1622.5
	Co	Co	Ta	Ta	Ta	1807.2
	Co	Ta	Co	Co	Co	− 963.7
	Co	Ta	Co	Co	Ta	− 1966.6
	Co	Ta	Co	Ta	Co	− 7970.6
	Co	Ta	Co	Ta	Ta	443.3
	Co	Ta	Ta	Co	Co	3377.9
	Co	Ta	Ta	Co	Ta	− 12,406.4
	Co	Ta	Ta	Ta	Co	11,814.0
	Co	Ta	Ta	Ta	Ta	− 1622.0
	Ta	Co	Co	Co	Co	8845.6
	Ta	Co	Co	Co	Ta	11,793.0
	Ta	Co	Co	Ta	Co	11,451.3
	Ta	Co	Co	Ta	Ta	24,253.6
	Ta	Co	Ta	Co	Co	− 13,822.6
	Ta	Co	Ta	Co	Ta	− 3787.2
	Ta	Co	Ta	Ta	Co	25,012.9
	Ta	Co	Ta	Ta	Ta	19,959.5
	Ta	Ta	Co	Co	Co	5796.1
	Ta	Ta	Co	Co	Ta	3283.0
	Ta	Ta	Co	Ta	Co	1968.8
	Ta	Ta	Co	Ta	Ta	990.7
	Ta	Ta	Ta	Co	Co	1967.7
	Ta	Ta	Ta	Co	Ta	− 11,092.4
	Ta	Ta	Ta	Ta	Co	27,645.7
	Ta	Ta	Ta	Ta	Ta	235.7

These were used to determine the total magnetic contribution to the Gibbs energy for the pure Co end-member, $^{\circ}G^{\mu}_{Co}$:

$$^{o}G^{\mu}_{Co} = \Delta G^{\mu}_{Co:Co:Co:Co:Co} - \Delta G^{\mu}_{Co,mag} + \Delta G^{HCP}_{Co,mag} + {}^{o}G^{HSER}_{Co} \quad (8)$$

where $G^{HCP}_{Co,mag}$ represents the magnetic contribution to the Gibbs energy of HCP Co, which is taken from SGTE database and is −8532 J/mol at 0 K. $^{\circ}G^{\mu}_{Co}$ was determined as 13,322 J/mol $+G^{HSER}_{Co}$; $^{\circ}G^{\mu}_{T\alpha}$ is obtained

Table 3
Enthalpies of formation, $\Delta G^{\phi}_{i:j:k:l}$ in J/mol (mole of atoms) for all configurations in four sublattice ordering of the BCC, FCC and HCP phases $\Delta G^{\phi}_{i:j:k:l:m}$.

Phase	Configuration				$\Delta G^{\phi}_{i:j:k:l}$
BCC	Co	Co	Co	Co	9522.5
	Ta	Co	Co	Co	1346.4
	Ta	Co	Ta	Co	7455.2
	Ta	Ta	Co	Co	− 9023.1
	Ta	Ta	Ta	Co	1448.5
FCC	Co	Co	Co	Co	1718.5
	Ta	Co	Co	Co	− 21,984.2
	Ta	Ta	Co	Co	− 11,511.8
	Ta	Ta	Ta	Co	15,467.6
	Ta	Ta	Ta	Ta	23,349.3
HCP	Co	Co	Co	Co	0.0
	Ta	Co	Co	Co	− 21,581.5
	Ta	Ta	Co	Co	17,122.7
	Ta	Ta	Ta	Co	18,279.6
	Ta	Ta	Ta	Ta	26,980.4

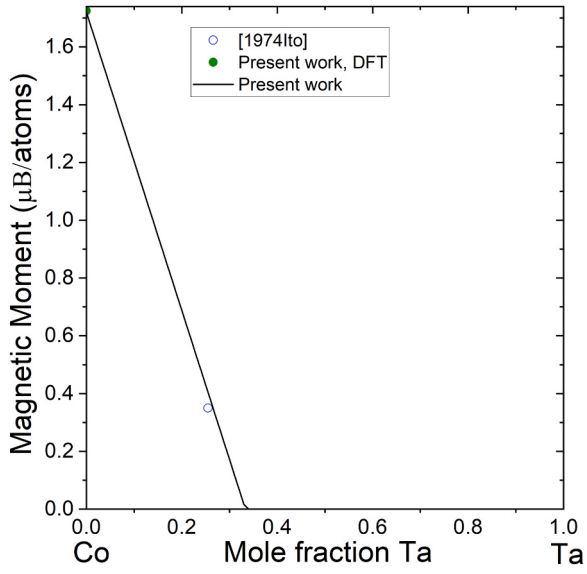

Fig. 1. Magnetic moment for the C36 phase.

from ${}^{o}G^{\mu}_{Ta} = \Delta G^{\mu}_{Ta:Ta:Ta:Ta} + G^{HSER}_{Ta}$ and is 10,458 J/mol $+G^{HSER}_{Ta}$. To reproduce the non-linear change in the average magnetic moment from the DFT calculations the magnetic contribution is added to the Gibbs energy of the pure Co end-member compound.

After that, all the A values of the $\Delta G^{\mu}_{i:j:k:l} = A + BT$ were evaluated by fitting the corresponding DFT values from present work using the modified CEF. B parameters were only introduced when they were necessary to obtain better agreement with the experimental phase diagram. A similar approach was applied to determine the Gibbs energies of the end-member compounds of the other TCP phases.

The DFT calculated magnetic moments for other TCP phases C14, C15 and C36 are similar to the one of the μ phase (Table 2) and were used as guide to estimate the Curie temperatures. For the pure Co end-member of the C36 phase the magnetic parameters are $TC^{C36}_{Co:Co:Co} = +1420$ K and $\beta^{C36}_{Co:Co:Co} = +1.72$ μ_B/atom. Fig. 1 shows the calculated magnetic moment for the C36 phase with experimental data from [23] and DFT result for pure Co in C36 structure. The present CALPHAD description reproduces the experimental data well. The calculation also shows that the magnetic contribution to the total energy for the C36 phase approaches 0 in its stable composition range. This also applies to the C14, C15 and μ phases. In fact, removing all magnetic parameters for C36, C15, C14 and μ phases does not make a significant difference in the calculated phase diagram. However,

Table 4
Phase names, models (sublattice formulae) and parameters of the present thermodynamic description. Gibbs energy is given in J/mol (mole of formula units according to the sublattice definition), temperature (T) in K.

Liquid: $(Co,Ta)_1$

$L^{0,Liquid}_{Co,Ta}$ = -141,864.9 + 38.5868·T; $L^{1,Liquid}_{Co,Ta}$ = -1803.2; $L^{2,Liquid}_{Co,Ta}$ = +11,722.5

(Ta) (BCC_A2): $(Co,Ta,Va)_1(Va)_3$

$G^{0,BCC_{A2}}_{Va:Va}$ = 30·T; $L^{0,BCC_{A2}}_{Co,Va:Va}$ = 46,912; $L^{0,BCC_{A2}}_{Ta,Va:Va}$ = 15,0000;

$L^{0,BCC_{A2}}_{Co,Ta:Va}$ = -55,308.6 + 11.8981·T; $L^{1,BCC_{A2}}_{Co,Ta:Va}$ = -31,039.5; $TC^{0,BCC_{A2}}_{Co,Ta}$ = 1450

(αCo)(γ) (FCC_A1): $(Co,Ta)_1(Va)_1$

$L^{0,FCC_{A1}}_{Co,Ta}$ = -78,885.0 + 10.5610·T; $L^{1,FCC_{A1}}_{Co,Ta}$ = +1945.8;

$TC^{0,FCC_{A1}}_{Co,Ta}$ = -2200; $TC^{1,FCC_{A1}}_{Co,Ta} = -804$; $\beta^{0,FCC_{A1}}_{Co,Ta} = 1.35$

(εCo) (HCP_A3):

$L^{0,HCP_{A3}}_{Co,Ta}$ = -47726.3

Co_3Ta: $(Co)_{0.7778}(Ta)_{0.2222}$

$\Delta G^{Co_3Ta}_f$ = -27,824.2 + 7.7303·T + 0.7778·$G^{HSER}_{Co}(T)$ + 0.2222·$G^{HSER}_{Ta}(T)$

μ: $(\mathbf{Co},Ta)_{0.07692}$ $(Co,\mathbf{Ta})_{0..30,769}$ $(Co,\mathbf{Ta})_{0.15385}$ $(\mathbf{Co},Ta)_{0.46154}$

${}^{\circ}G^{\mu}_{Co}$ = +13,322 +$G^{HSER}_{Co}(T)$;; ${}^{\circ}G^{\mu}_{Ta}$ = +10,456.5 +$G^{HSER}_{Ta}(T)$; ${}^{\circ}G^{0,\mu}_{Co,Ta}$ = +20,511.2;

$\Delta G^{\mu}_{Co:Co:Co:Co}$ = 0; $TC^{\mu}_{Co:Co:Co:Co}$ = 1460; $\beta^{\mu}_{Co:Co:Co:Co}$ = 1.76;

$\Delta G^{\mu}_{Ta:Co:Co:Co}$ = -11650;

$\Delta G^{\mu}_{Co:Ta:Co:Co}$ = -38,941.4 + 2.5000·T; $\Delta G^{\mu}_{Ta:Ta:Co:Co}$ = -18,258;

$\Delta G^{\mu}_{Co:Co:Ta:Co}$ = -10,780; $\Delta G^{\mu}_{Ta:Co:Ta:Co}$ = -13,840;

$\Delta G^{\mu}_{Co:Ta:Ta:Co}$ = -44,989.6 + 3.0882·T; $\Delta G^{\mu}_{Ta:Ta:Ta:Co}$ = -46,589.3 + 5.0752·T;

$\Delta G^{\mu}_{Co:Co:Co:Ta}$ = +26,036; $\Delta G^{\mu}_{Ta:Co:Co:Ta}$ = +38,781; $\Delta G^{\mu}_{Co:Ta:Co:Ta}$ = +9041;

$\Delta G^{\mu}_{Ta:Ta:Co:Ta}$ = +14,471; $\Delta G^{\mu}_{Co:Co:Ta:Ta}$ = +35,800; $\Delta G^{\mu}_{Ta:Co:Ta:Ta}$ = +46,388;

$\Delta G^{\mu}_{Co:Ta:Ta:Ta}$ = -4936; $\Delta G^{\mu}_{Ta:Ta:Ta:Ta}$ = 0

C36: $(Co,Ta)_{0.3333}(Co,Ta)_{0.1667}(Co,Ta)_{0.5000}$

$G^{C36}_{Co:Co:Co}$ = +19,113.7 +$G^{HSER}_{Co}(T)$; $TC^{C36}_{Co:Co:Co}$ = +1420; $\beta^{C36}_{Co:Co:Co}$ = +1.72;

$G^{C36}_{Ta:Co:Co}$ = -27691.8 + 4.3938·T + 0.6667·$G^{HSER}_{Co}(T)$ + 0.3333·$G^{HSER}_{Ta}(T)$;

$G^{C36}_{Co:Ta:Co}$ = +11,796 + 0.8333·$G^{HSER}_{Co}(T)$ + 0.1667·$G^{HSER}_{Ta}(T)$;

$G^{C36}_{Ta:Ta:Co}$ = -21,027.2 + 0.5·$G^{HSER}_{Co}(T)$ + 0.5·$G^{HSER}_{Ta}(T)$;

$G^{C36}_{Co:Co:Ta}$ = +39,100 + 0.5·$G^{HSER}_{Co}(T)$ + 0.5·$G^{HSER}_{Ta}(T)$;

$G^{C36}_{Ta:Co:Ta}$ = +213.6 + 0.1667·$G^{HSER}_{Co}(T)$ + 0.8333·$G^{HSER}_{Ta}(T)$;

$G^{C36}_{Co:Ta:Ta}$ = +71,002.4 + 0.3333·$G^{HSER}_{Co}(T)$ + 0.6667·$G^{HSER}_{Ta}(T)$;

$G^{C36}_{Ta:Ta:Ta}$ = +10,485.5 +·$G^{HSER}_{Ta}(T)$;

$G^{C36}_{Co,Ta:Co:Co}$ = -39,910.6 + 5.8085·T;

C15 $(Co,Ta)_{0.667}(Co,Ta)_{0.333}$

$G^{C15}_{Co:Co}$ = +21,045.6 +$G^{HSER}_{Co}(T)$; $TC^{C15}_{Co:Co}$ = +1440; $\beta^{C15}_{Co:Co}$ = +1.73;

$G^{C15}_{Ta:Co}$ = 69,432 + 0.333·$G^{HSER}_{Co}(T)$ + 0.667·$G^{HSER}_{Ta}(T)$;

$G^{C15}_{Co:Ta}$ = -28,158.3 + 3.5524·T + 0.667·$G^{HSER}_{Co}(T)$ + 0.333·$G^{HSER}_{Ta}(T)$;

$G^{C15}_{Ta:Ta}$ = +11,165.5 +$G^{HSER}_{Ta}(T)$;

$G^{C15}_{Co:Co,Ta}$ = -46,121.7 + 13.8435·T

C14 $(Co,Ta)_{0.3333}(Co,Ta)_{0.1667}(Co,Ta)_{0.5000}$

$G^{C14}_{Co:Co:Co}$ = +17,801.3 +$G^{HSER}_{Co}(T)$; $TC^{C14}_{Co:Co:Co}$ = +1400; $\beta^{C14}_{Co:Co:Co}$ = +1.71;

$G^{C14}_{Ta:Co:Co}$ = -28,175.8 + 3.6946·T + 0.6667·$G^{HSER}_{Co}(T)$ + 0.3333·$G^{HSER}_{Ta}(T)$;

$G^{C14}_{Co:Ta:Co}$ = +10,326.4 + 0.8333·$G^{HSER}_{Co}(T)$ + 0.1667·$G^{HSER}_{Ta}(T)$;

$G^{C14}_{Ta:Ta:Co}$ = -26,426.4 + 5.0199·T + 0.5·$G^{HSER}_{Co}(T)$ + 0.5·$G^{HSER}_{Ta}(T)$;

$G^{C14}_{Co:Co:Ta}$ = +40,221 + 0.5·$G^{HSER}_{Co}(T)$ + 0.5·$G^{HSER}_{Ta}(T)$;

$G^{C14}_{Ta:Co:Ta}$ = -147 + 0.1667·$G^{HSER}_{Co}(T)$ + 0.8333·$G^{HSER}_{Ta}(T)$;

$G^{C14}_{Co:Ta:Ta}$ = +74,473 + 0.3333·$G^{HSER}_{Co}(T)$ + 0.6667·$G^{HSER}_{Ta}(T)$;

$G^{C14}_{Ta:Ta:Ta}$ = +9670.3 +·$G^{HSER}_{Ta}(T)$

C16 $(Co,Ta)_{0.333}$ $(Co,Ta)_{0.667}$

$G^{C16}_{Co:Co}$ = +40,568 +$G^{HSER}_{Co}(T)$;

$G^{C16}_{Ta:Co}$ = +18,617 + 0.333·$G^{HSER}_{Ta}(T)$ + 0.667·$G^{HSER}_{Co}(T)$;

$G^{C16}_{Co:Ta}$ = -25500 + 5.4763·T + 0.333·$G^{HSER}_{Co}(T)$ + 0.667·$G^{HSER}_{Ta}(T)$;

$G^{C16}_{Ta:Ta}$ = +48,196 +$G^{HSER}_{Ta}(T)$;

$G^{C16}_{Co:Co,Ta}$ = -63,064.7;

$G^{C16}_{Co,Ta:Ta}$ = -18,333.5–14.61·T

$L1_2$ $(Co,Ta)_{0.25}(Co,Ta)_{0.25}(Co,Ta)_{0.25}(Co,Ta)_{0.25}$

CEF order/disorder formalism [30]

u_{AB} = -9163.2 + 5.9565·T; $\Delta G^{L1_2}_{Co_3Ta} = 3\,u_{AB}$; $\Delta G^{L1_2}_{Co_2Ta_2} = 4\,u_{AB}$ + 25,652.8;

$\Delta G^{L1_2}_{CoTa_3} = 3\,u_{AB}$ + 42,489.6 – 17.8695 T = 15,000

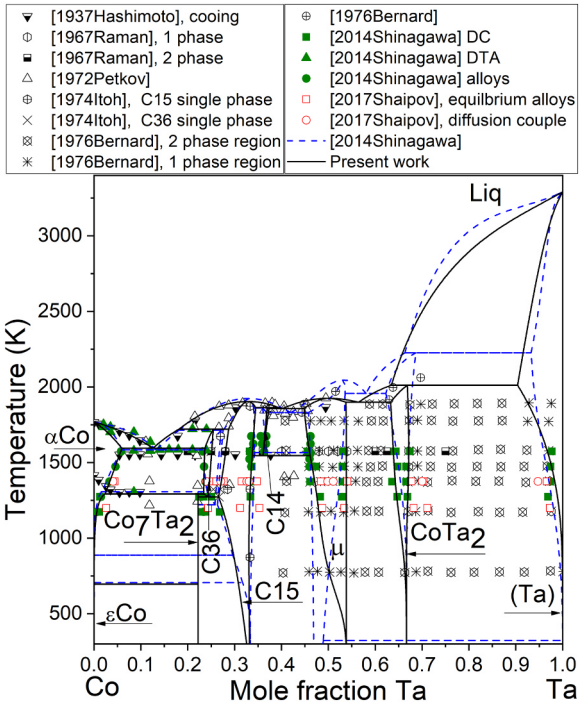

Fig. 2. Calculated Co-Ta phase diagram compared with experimental data.

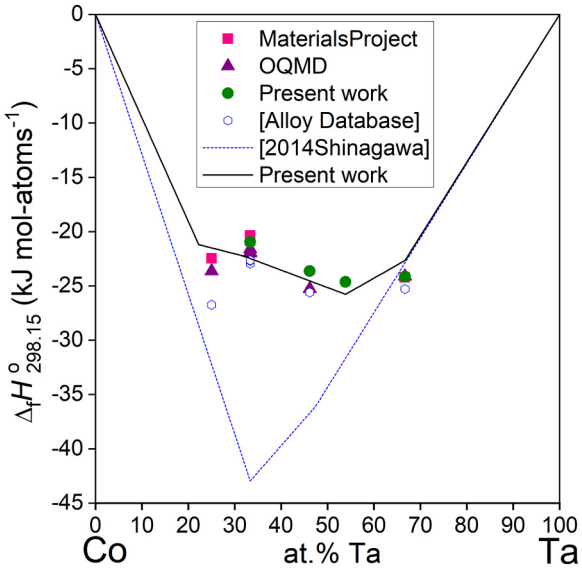

Fig. 3. Calculated enthalpies of formation of the solid phases in the Co-Ta system at 298.15 K compared with DFT results at 0 K.

considering the magnetic contribution to the total Gibbs energy for the determination of the parameters of the end-member compounds is important. The Gibbs energies of formation of the pure Co endmember phases without magnetic contribution is noticeably higher. For example, for the μ phase this value increases from 11,252 J/mol to 13,322 J/mol. The contribution of the magnetism to the Gibbs energy declines with increasing temperature but nevertheless affects the calculated phase diagram also at temperatures above Curie temperature. Therefore, the magnetic contribution to the Gibbs energy should be considered. We pointed out in our previous work [38] that proper treatment of the magnetism is essential for an accurate description of the phases in Co systems.

We find that treatment of the magnetic contribution to the energy in Co-Ta is mainly important for Co mole fractions of more than

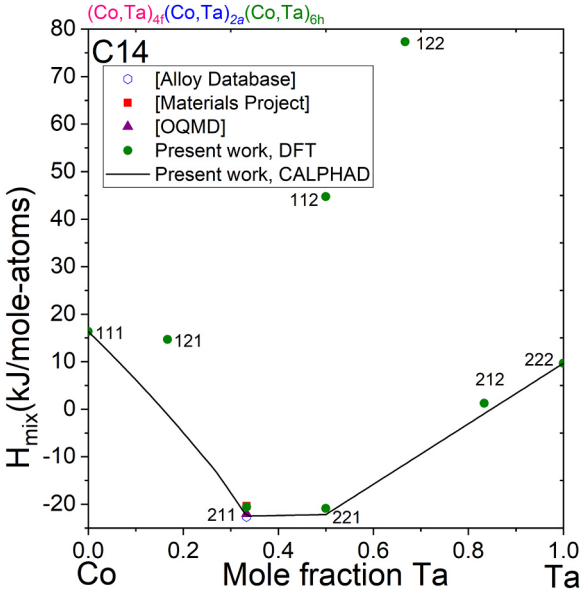

Fig. 4. Calculated enthalpy of formation for the C14 phase at 298.15 K compared with the DFT results for all end-members at 0 K.

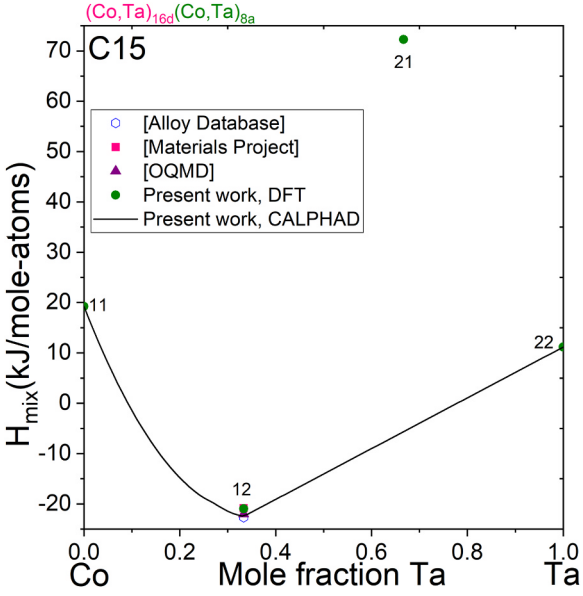

Fig. 5. Calculated enthalpy of formation for the C15 phase at 298.15 K compared with the DFT results for all end-members at 0 K.

approximately 75%, as it was shown in Fig. 1 for the calculated magnetic moment of the C36 phase. 1. A similar range was observed in DFT calculations for the isoelectric Co-V and Co-Nb systems [30].

5. CALPHAD results

The optimization of the model parameters of the Co-Ta system was performed using the PARROT module of the Thermo-Calc software [40]. Table 4 lists the phases, names, models, and parameters used in the present work.

The calculated Co-Ta phase diagram is shown in Fig. 2, it agrees with the majority of the experimental data except the ones from Shaipov et al. [24]. It can be seen in Fig. 2 that the experimental results from Shaipov et al. [24] from the diffusion couple (red circles) and the annealed alloys (red squares) are not consistent with each other and, therefore, these data were not used for the parameter optimization. It is

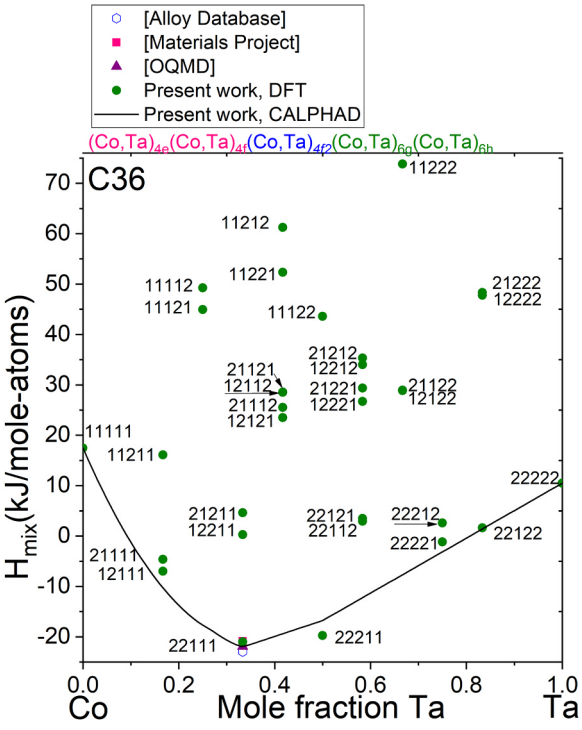

Fig. 6. Calculated enthalpy of formation for the C36 phase at 298.15 K compared with the DFT results for all end-members at 0 K.

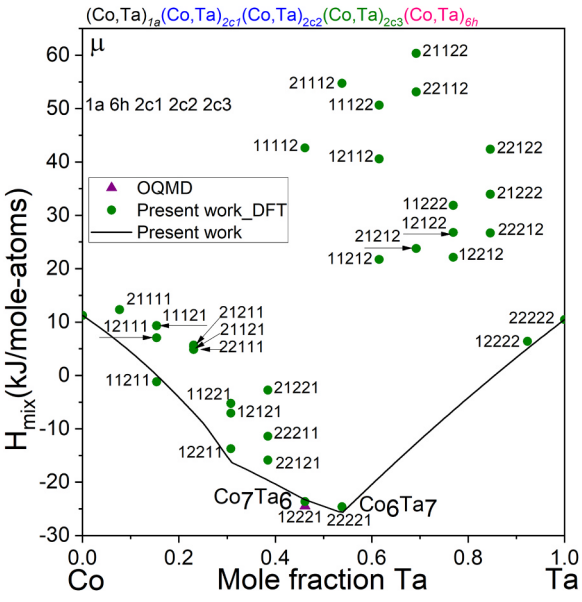

Fig. 7. Calculated enthalpy of formation for the μ phase at 298.15 K compared with the DFT results for all end-members at 0 K.

almost impossible to experimentally determine the homogeneity range for the μ phase at low temperatures, e.g., below 900 K. The present DFT calculations show that the Co_6Ta_7 is more stable than Co_7Ta_6. This is also reflected by the CALPHAD calculation that shows that the stable composition range for the μ phase at room temperature is close to Co_6Ta_7 instead of Co_7Ta_6.

Fig. 3 shows the calculated enthalpy of formation at 298.15 K compared to results from the present DFT calculations and DFT databases [41–46]. The results from the present CALPHAD description agree well with the DFT results while the enthalpies calculated with the description from Shinagawa et al. [12] show deviations that are

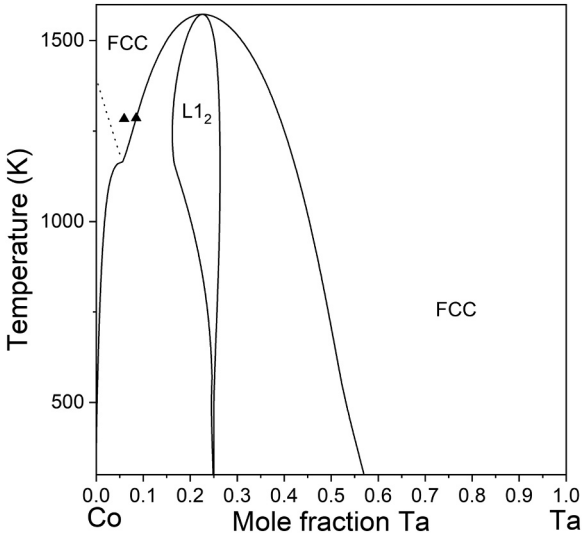

Fig. 8. Calculated metastable FCC-$L1_2$ phase diagram compared with the FCC-L12 solvus temperatures from [12].

significantly larger. The DFT data points at x(Ta) = 0.3333 are the formation energies of the C36, C15 and C14 phases while for the CALPHAD calculation only the stable phase at 298 K, C15, was considered. Figs. 4–7 show the calculated enthalpies of formation for the C14, C15, C36 and μ phases at 298.15 K compared with the DFT results. For the C14 phase, each end-member is presented by a three-digit number, e.g., 211, where 1 corresponds to Co and 2 to Ta, and the order of digits reflect the occupancy of the corresponding sublattices in the following order: Ta(4*f*)-Co(2*a*)-Co(6*h*), i.e., 211 corresponds to $Ta_4Co_2Co_6$. The same syntax is used to identify the end-members of the C14, C36, and μ phases in Figs. 5–7. It can be seen from these figures that the present CALPHAD description captures the DFT results well.

For the description of the metastable ordering of the FCC phase the DFT values were adapted. FCC-$L1_2$ solvus temperatures from [12] were used to evaluate the temperature dependent terms. The metastable FCC-$L1_2$ phase diagram is shown in Fig. 8. More theoretical and experimental studies for the FCC-$L1_2$ phase equilibria are needed to obtain a more reliable description of the $L1_2$ phase.

6. Conclusions

A critical review of the available CALPHAD descriptions for the Co-Ta system showed that a thermodynamic re-assessment of the Co-Ta system was necessary.

DFT calculations were performed to obtain the energies for all possible end configurations of the intermetallic phases C14, C15, C36 and μ phases considering spin polarization. These results were used to evaluate the Gibbs energies for all the end-members of these phases. It was found that it is essential to consider the magnetic contribution to the total Gibbs energy for complex compounds with Co even if these compounds do not show magnetism in their stable composition ranges. The Gibbs energy differences resulting for the magnetic contribution are significant enough to make a difference in the calculated phase diagram signifying the importance of proper consideration of the magnetic contribution to the total energy.

The phase diagram calculated with the present CALPHAD description agrees well with the experimental data. The results from the DFT calculations were essential for improving the descriptions of the TCP phases, particularly that of the μ phase to give realistic phase equilibria at lower temperatures.

Acknowledgement

We thank Dr. Suzana G. Fries for helpful discussions. This work was performed under the following financial assistance award 70NANB14H012 from U.S. Department of Commerce, National Institute of Standards and Technology as part of the Center for Hierarchical Materials Design (CHiMaD). JK, MP, and TH acknowledge funding by the Deutsche Forschungsgemeinschaft (DFG) through projects C1 and C6 of the collaborative research centre SFB/TR 103.

Appendix A. Supplementary material

Supplementary data associated with this article can be found in the online version at doi:10.1016/j.calphad.2018.12.002.

References

[1] A.J.A. Mom, 1 - Introduction to gas turbines, in: P. Jansohn (Ed.), Modern Gas Turbine Systems, Woodhead Publishing, Cambridge, 2013, pp. 3–20.
[2] T.M. Pollock, J. Dibbern, M. Tsunekane, J. Zhu, A. Suzuki, New Co-based γ-γ′ high-temperature alloys, JOM 62 (2010) 58–63.
[3] J. Sato, T. Omori, K. Oikawa, I. Ohnuma, R. Kainuma, K. Ishida, Cobalt-base high-temperature alloys, Science 312 (2006) 90–91.
[4] A. Suzuki, H. Inui, T.M. Pollock, $L1_2$-strengthened cobalt-base superalloys, Annu. Rev. Mater. Res. (2015).
[5] K. Ishida, Intermetallic Compounds in Co-base Alloys–phase Stability and Application to Superalloys, Cambridge Univ Press, 2008 (1128-U1106-1106),(MRS Proc).
[6] J. Koßmann, T. Hammerschmidt, S. Maisel, S. Müller, R. Drautz, Solubility and ordering of Ti, Ta, Mo and W on the Al sublattice in $L1_2$-Co_3Al, Intermetallics 64 (2015) 44–50.
[7] B. Seiser, T. Hammerschmidt, A. Kolmogorov, R. Drautz, D. Pettifor, Theory of structural trends within 4 d and 5 d transition metal topologically close-packed phases, Phys. Rev. B 83 (2011) 224116.
[8] G.B. Olson, Preface to the viewpoint set on: the materials genome, Scr. Mater. 70 (2014) 1–2.
[9] P. Villars, Pearson's Handbook: Desk Edition: Crystallographic Data for Intermetallic Phases, ASM international, Materials Park, OH, 1997.
[10] Z.-K. Liu, Y.A. Chang, Thermodynamic assessment of the Co-Ta system, Calphad 23 (1999) 339–356.
[11] K.C. Hari Kumar, T. Van Rompaey, P. Wollants, Thermodynamic calculation of the phase diagram of the Co-Nb-Ta system, Z. Metallkd. 93 (2002) 1146–1153.
[12] K. Shinagawa, H. Chinen, T. Omori, K. Oikawa, I. Ohnuma, K. Ishida, R. Kainuma, Phase equilibria and thermodynamic calculation of the Co-Ta binary system, Intermetallics 49 (2014) 87–97.
[13] U. Haschimoto, Relation between the allotropic transformation of cobalt and some additional elements, J. Jpn Inst. Met. 1 (1937) 177–190.
[14] W. Köster, W. Mulfinger, The alloys of cobalt with boron, arsenic, zirconium, columbium and tantalum, Z. Metallkd. 30 (1938) 348–350.
[15] M. Korchynsky, R.W. Fountain, Precipitation phenomena in cobalt-tantalum alloys, Trans. Met. Soc. 215 (1959) 1033–1043.
[16] R. Dragsdorf, W. Foreing, The intermetallic phases in the cobalt-tantalum system, Acta Crystallogr. 15 (1962) 531–536.
[17] J. Ponsioen, J. Van Vucht, The Structure of β-$TaCo_3$ and the Effect of the Substitution of Ta and Co by Related Elements, Philos. Res. Rep. 22 (1967) 161–169.
[18] A. Raman, X-ray examination of the Ta-Co system, Metal 21 (1967) 900–903.
[19] V.V. Pet'kov, Y.A Kocherzhinskii, V.У Markiv, Phase diagram of the tantalum-cobalt system, Metallofizika 41 (1972) 93–97.
[20] H. Xu, X. Xiong, Y. Du, P. Wang, B. Hu, Y. He, Phase equilibria of the Co-Ta-Ti system at 950 °C, J. Alloy. Compd. 485 (2009) 249–254.
[21] V.B. Bernard, L.A. Yurchenko, O.I. Bodak, V.V. Kuprina, Study of the Phase Diagram of the Tantalum-cobalt System, Vestn Mosk Univ, Ser 2: Khim, 1976, pp. 208–212.
[22] T.B. Massalski, H. Okamoto, P.R. Subramanian, L. Kacprzak, Binary Alloy Phase Diagrams, 2nd ed., ASM International, Materials Park, OH, 1990.
[23] H. Itoh, Y. Aoki, T. Nakamichi, M. Yamamoto, Crystal structures, homogeneity ranges and magnetic properties of tantalum-cobalt laves phases, Z. Metallkd. 65 (1974) 149–157.
[24] R.K. Shaipov, E.Y. Kerimov, E.M. Slyusarenko, Isothermal sections of the Co-Ni-Ta phase diagram at 1200 and 1375 K, J. Alloy. Compd. 701 (2017) 262–278.
[25] Scientific Group Thermodata Europe: SGTE, ⟨https://www.sgte.net/en/free-pure-substance-database⟩, visited 21-June-2018.
[26] A.T. Dinsdale, SGTE data for pure elements, Calphad 15 (1991) 317–425.
[27] O. Redlich, A.T. Kister, Algebraic representation of thermodynamic properties and the classification of solutions, Ind. Eng. Chem. 40 (1948) 345–348.
[28] M. Hillert, M. Jarl, A model for alloying in ferromagnetic metals, Calphad 2 (1978) 227–238.
[29] M. Hillert, The compound energy formalism, J. Alloy. Compd. 320 (2001) 161–176.
[30] T. Hammerschmidt, A.F. Bialon, D.G. Pettifor, R. Drautz, Topologically close-packed phases in binary transition-metal compounds: matching high-throughput ab initio calculations to an empirical structure map, New J. Phys. 15 (2013) 115016.
[31] I. Ansara, B. Burton, Q. Chen, M. Hillert, A. Fernandez-Guillermet, S.G. Fries, H.L. Lukas, H.-J. Seifert, W.A. Oates, Models for composition dependence, Calphad 24 (2000) 19–40.
[32] A. Kusoffsky, N. Dupin, B. Sundman, On the compound energy formalism applied to fcc ordering, Calphad 25 (2001) 549–565.
[33] G. Kresse, J. Hafner, Ab initio molecular-dynamics simulation of the liquid-metal-amorphous-semiconductor transition in germanium, Phys. Rev. B 49 (1994) 14251–14269.
[34] G. Kresse, J. Furthmüller, Efficient iterative schemes for ab initio total-energy calculations using a plane-wave basis set, Phys. Rev. B 54 (1996) 11169–11186.
[35] P.E. Blöchl, O. Jepsen, O.K. Andersen, Improved tetrahedron method for Brillouin-zone integrations, Phys. Rev. B 49 (1994) 16223.
[36] J.P. Perdew, K. Burke, M. Ernzerhof, Generalized gradient approximation made simple, Phys. Rev. Lett. 77 (1996) 3865.
[37] H.J. Monkhorst, J.D. Pack, Special points for Brillouin-zone integrations, Phys. Rev. B 13 (1976) 5188–5192.
[38] P. Wang, M.C. Peters, U.R. Kattner, K. Choudhary, G.B. Olson, Thermodynamic analysis of the topologically close packed σ phase in the Co-Cr system, Intermetallics 105 (2019) 13–20.
[39] A.I. Liechtenstein, M. Katsnelson, V. Antropov, V. Gubanov, Local spin density functional approach to the theory of exchange interactions in ferromagnetic metals and alloys, J. Magn. Magn. Mater. 67 (1987) 65–74.
[40] Thermo-Calc Software, ⟨http://www.thermo-calc.com⟩, visited 21-June-2018.
[41] Alloy Database, ⟨http://alloy.phys.cmu.edu/⟩, visited 21-June-2018.
[42] The Materials Project, ⟨https://materialsproject.org/⟩, visited 21-June-2018.
[43] OQMD: The Open Quantum Materials Database, ⟨http://oqmd.org/⟩, visited 21-June-2018.
[44] J.E. Saal, S. Kirklin, M. Aykol, B. Meredig, C. Wolverton, Materials design and discovery with high-throughput density functional theory: the open quantum materials database (OQMD), JOM 65 (2013) 1501–1509.
[45] S. Kirklin, J.E. Saal, B. Meredig, A. Thompson, J.W. Doak, M. Aykol, S. Rühl, C. Wolverton, The open quantum materials database (OQMD): assessing the accuracy of DFT formation energies, NPJ Comput. Mater. 1 (2015) 15010.
[46] A. Jain, S.P. Ong, G. Hautier, W. Chen, W.D. Richards, S. Dacek, S. Cholia, D. Gunter, D. Skinner, G. Ceder, K.A. Persson, Commentary: the materials project: a materials genome approach to accelerating materials innovation, APL Mater. 1 (2013) 011002.